Available online at www.sciencedirect.com
SCIENCE DIRECT®
Journal of Geodynamics 37 (2004) 103–124
JOURNAL OF GEODYNAMICS
www.elsevier.com/locate/jog

One My scale subsidence of carbonate sedimentary bodies and the viscosity of the lower crust

Pascal Allemand[a,*], Gilles Dromart[b], Jean-Pierre Garcia[c], Fabrice Gaumet[d], Cécile Robin[e]

[a]*Université Claude Bernard Lyon 1, 2 rue Raphaël Dubois, UMR CNRS 5570, 69622 Villeurbanne Cedex, France*
[b]*Université Claude Bernard Lyon 1, 2 rue Raphaël Dubois, UMR CNRS 5125, 69622 Villeurbanne Cedex, France*
[c]*Université de Bourgogne, UMR CNRS 5561, 21000 France*
[d]*IFP, BP 311, 92506 Rueil-Malmaison Cedex, France*
[e]*Université P. et M. Curie Paris 6, ESA 7073, case postale 116, 75252 Paris Cedex 05, France*

Received 14 January 2003; received in revised form 11 August 2003; accepted 10 September 2003

Abstract

The possibility of flow of the lower crust under the load produced by carbonate sedimentary accumulations is investigated through the example of the Paris basin during the Middle Jurassic (i.e. Bathonian). Depositional geometries, water depths and sedimentary environments have been estimated and correlated for 164 sites spread over a surface of 380 per 220 km for three successive periods lasting each less than 0.8 My. A signal of relative vertical displacement has been extracted from water-depth and sedimentary thickness. Data have then been interpolated to produce maps of velocity of vertical displacement, sedimentation rate, water depth, and water-depth variation between two periods. The maps show that the western part of the basin is affected by faults which are independent of the sedimentation. The eastern part of the basin consists of a shallow carbonate platform affected by diffuse subsidence patches which are positively correlated with sedimentation. The patches of diffuse subsidence are elliptic in shape, with a radius of 20 km, a mean thickness of 40 m, and a maximum elevation of 10 m above the surrounding sea bottom. We suggest that the load of these patches induces the flow of the lower crust. The topography produced by these patches would be maintained at steady state by in situ carbonate production/accumulation combined with the lower crust flow. This model is tested by estimating the viscosity and the thickness of the flowing crust necessary to meet the geometric and kinematic conditions obtained from the patches. This model is valid for a lower crust viscosity of around 10^{21} Pa s. This value is higher by one order of magnitude than those inferred from other contexts but can be explained by the influence on viscosity of the load and temperature for a non-newtonian rock rheology.

* Corresponding author. Fax: +33-4-7244-8593.
E-mail address: allemand@univ-lyon1.fr (P. Allemand).

0264-3707/$ - see front matter © 2003 Elsevier Ltd. All rights reserved.
doi:10.1016/j.jog.2003.09.001

1. Introduction

Lithospheric strength profiles show that generally the lower crust is a weak viscous channel sandwiched between two resistant, possibly brittle, layers which are the upper mantle and the intermediate crust (e.g. Ranalli and Murphy, 1987). The effects of this viscous channel on tectonic processes have been suggested for a wide range of time scales. For long term tectonic processes such as rift development and mountain building (time scale exceeding 5 My), numerical models have revealed the sensitivity of the lower crust flow to pressure gradients generated by topography (e.g. Buck, 1991; Hopper and Buck, 1996; Burov and Cloetingh, 1997; McKenzie et al., 2000) and have pointed out possible feedback mechanisms between erosion and collision processes through this weak channel (e.g. Avouac and Burov, 1996). Flow of the lower crust has also been suggested from geological data obtained in the Basin and Range province (Kruse at al., 1991; Kaufman and Royden, 1994; Bills et al., 1994; McCready et al., 1997; McQuarrie and Rodgers, 1998) to explain spatial and temporal evolution of subsidence or to explain uniformity of gravity and topography between extended and non-extended adjacent regions. Data collected from these works are compatible with an effective viscosity of the lower crust ranging from 10^{18} to 10^{20} Pa s. On an intermediate time scale of 1–5 My, the flow of the lower crust could be important after the emplacement of granitic bodies in the upper crust (Bott, 1999). For short time scales (less than 10 ky), the flow of the lower crust participates to stress relaxation of post-seismic events (Rydelek and Sacks, 1990; Deng et al., 1998), to isostatic adjustment related to human activity (i.e. mining; Klein et al., 1997), and to topographic relaxation after the melting of ice caps (e.g. Klemann and Wolf, 1999).

Time lines bounding carbonate sedimentary bodies can be delineated under a resolution of several 100 ky (Garcia and Dromart, 1997; Dromart et al., 2002). This time scale is intermediate between that of geodynamic processes acting at the velocity of plate tectonics and that of climatic or human driven processes. For a newtonian viscosity, the time constant of the lower crust flow driven by a surface load is given by (Lliboutry, 1976) (see Table 1 for the explanation of the symbols):

$$\tau = \frac{4\eta}{\rho g H^3 k^2} \tag{1}$$

For a mean viscosity of the crust of 10^{20} Pa s, a density of 2700 kg m^{-3}, a thickness of the crustal channel of 15 km and a surface load with a wave number of 3.10^{-5} m^{-1} (wavelength of about 100 km), the time constant of the system is around 100 ky (Fig. 1). The characteristic times of sedimentary construction and lower crustal flow are then similar. The flow of the lower crust should thus be instrumental in the control of the geometry of sedimentary bodies. However, the possible interplay between the two processes is generally masked by the brittle tectonics associated with the horizontal displacements, and is difficult to observe because of the high time resolution which is needed for the delineation of sedimentary bodies. Such a signal has to be sought in sedimentary environments for which horizontal tectonics is low enough. This approach can be realized successfully on intracontinental basins (ICB) which are circular structures with a diameter of several hundred km. ICB subsidence typically exceeds 150 My in duration, with velocities lower than 50 m My^{-1} on average. ICB are generally affected by few normal faults. The amount of extension is low and the thinning of the crust is low to nil (Pinet and Coletta, 1990; Stel et al., 1993).

Table 1
Symbols used in flow equations

g	Gravity
ρ_c	Density of crust and sediments
ρ_w	Density of water
η	Viscosity of the lower crust
H	Thickness of the lower crust
k	Wave number of the load
λ	Wave length of the topography
l	e^{Hk}
Uf	Horizontal velocity of the flow in the lower crust
Vf	Vertical velocity of the flow in the lower crust
Vs	Difference of sedimentation velocity between the patch and the rest of the platform
E	Topography
q	Load applied at the surface
σ	Deviatoric stress
Q	Activation energy
R	Universal gas constant
T	Absolute temperature
N	Exponential factor
M	Pre-exponential term

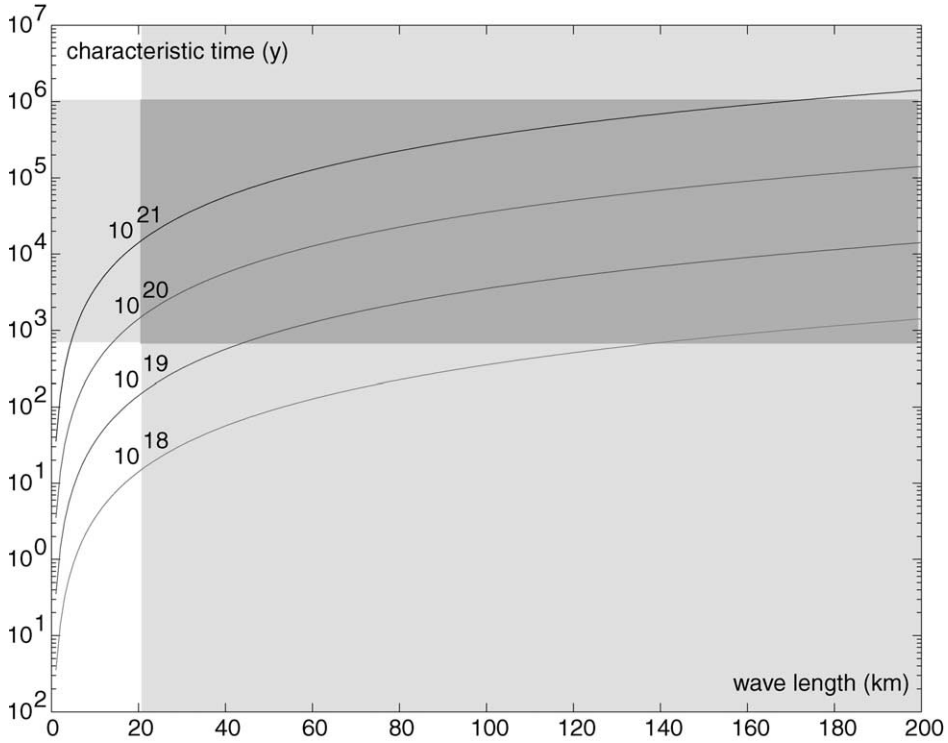

Fig. 1. Characteristic times of the flow in the lower crust (from Lliboutry, 1976). The characteristic time is in the same range as the life span of a sedimentary body.

The paper aims at investigating the possible effects of the building up of carbonate sedimentary bodies on the flow of the lower crust in the Paris basin during the Bathonian. Maps of subsidence velocities have been extracted from a stratigraphic data-base containing information on age, sedimentary thickness and depositional water-depth of 164 sites in the Paris basin for three successive periods each lasting less than 0.8 My. The geometrical and temporal characteristics of sedimentary bodies have been tested against a model of flow of the lower crust. This study concludes that these characteristics are compatible with the flow of a crust having a effective viscosity of about 10^{21} Pa s.

2. Geological setting

The Middle Jurassic of western Europe is characterized by significant sediment accumulation (Fig. 2a). Specifically, the Bathonian carbonate platforms of the Paris Basin show a vertical development of about 100 m in the western margin to 300 m in the basin. Major faults inducing topographic highs and subsiding zones crossed the basin at that time (Fig. 2a). In the Bathonian, the Paris basin was occupied by carbonate shoals, fringing emerged land areas (Armorican, London-Brabant, Massif central Highs), and offshore domains (Ziegler, 1988). The Bathonian series are incorporated into an overall stratigraphic cycle (Garcia et al., 1996; Gaumet, 1997)

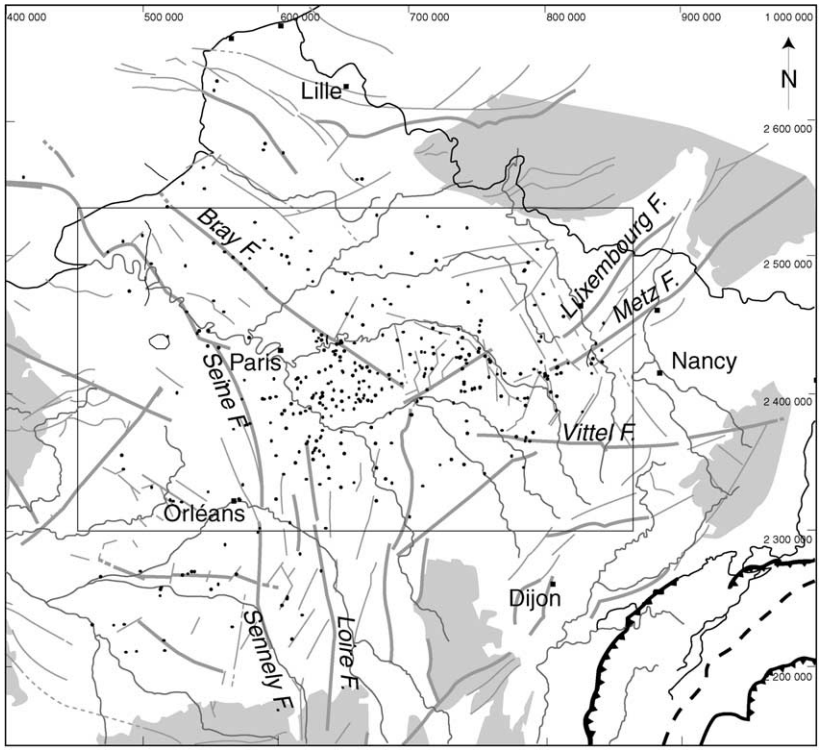

Fig. 2. Map of the Paris basin showing the position of the 164 investigated wells, and the main brittle structures affecting the area. The map is in Lambert II projection. The studied area is delimitated by the rectangle.

composed of (1) a regressive hemicycle from the Upper Bajocian to the Lower/Middle Bathonian boundary which corresponds to an overall infill of the basin associated with the progradation of carbonate deposits ultimately conducting to subaerial exposure, and (2) a transgressive hemicycle from the Middle Bathonian up to the marine flooding of middle Callovian age when residual shallow carbonate deposits stacked on topographic highs were drowned by offshore deposits.

3. Data set and preprocessing

Most of the data-base relative to the Bathonian-Callovian of the Paris basin comes from the subsurface (cores and well-logs) in association with the extensive oil exploration conducted all over the basin since 1958. Additional information derives from outcrops located all around the basin (Normandy Coast; Burgundy). A set of 164 sites distributed over a surface of around 83,000 km^2 (380 per 220 km) has been processed. Site distribution and spacing are fairly regular even if the southwestern basin is marked by the scarcity of boreholes due to the lack of subsurface hydrocarbon reservoirs.

3.1. Stratigraphic correlations

The depositional geometries were restored by constructing a web network of stratigraphic cross-sections all over the study area. The cross-sections were correlated in the case of carbonate platforms by using the lithologic markers of marine flooding occurrences. The method used is somewhat similar to the procedure applied by Underhill and Partington (1993) in the Jurassic of the North-Sea. Since most of the data come from the subsurface, cross-sections derive from the correlation of well-logs. Marine flooding events usually correspond to shaley deposits which can be tracked through inspection of conventional well-logs, i.e. combinations of positive excursions of the Gamma-Ray log with negative deflections of Neutron and Sonic logs in response to increasing porosity (Table 2).

Additionally, there is control of the sedimentological significance (i.e., lithology, depositional facies and environment) of the well-log patterns. This is done by comparing core and well-log data available through the same interval of a well or a pair of wells, e.g., BTS 001 and CS 001 wells (Fig. 3). This calibration procedure leads to the identification of a series of prominent well-log markers (0–34; Fig. 2b). Subsequently, a grid of stratigraphic cross-sections is achieved by correlating wells one by one (Fig. 2b; Garcia and Dromart, 1997). The correlation does not refer to any a priori stratigraphic model (e.g., volumetric partitioning of sediments) but is based on the recognition, and the correlation, of particular and recurrent sedimentological markers (i.e., marine floodings). The shape of well-log deflections marking those marine flooding events changes from site to site. A gradual change allows reliable time-lines to be drawn whereas a total fading of the well-log marker will cause the correlation-line to be omitted (Fig. 2b). Finally, well-log markers may split into a number of subordinate markers that further merge, with the possibility of incorporating extra-markers coming from above or below in the stratigraphic column. In that case, time-lines obtained from the well-log correlation are moderately constrained and the possible drift of the correlation may attain a limited magnitude of a few meters throughout the basin. Moreover, the robustness of correlation is confidently tested by biostratigraphic data

Table 2
Calibration of depositional environments and related water depths against well-logs for the Middle Jurassic of the Paris Basin a

Depositional environment (core data)	Gamma-ray A.P.I.	Lithodensity (PEF) barn/electron	Neutron (NPHI)/ density (RHOB) deviation (no unit)	Resistivity log (Ohm m^2/m)	Sonic (μs/foot)	Water depth (m)
Shoreface	5–20	4.5–6	0	2–150	60–75	<20
Inner upper offshire Offshore	15–40	4.5–5.5	0–0.5	10–100	50–75	20–50
Middle-Outer Upper offshore	15–75	2.0–5.5	1.2–2	10–100	50–90	50–110
Lower offshore	50–105	1.5–2.5	1.8–2.7	1–6	90–110	>110

Ranges for well-logs correspond to end-member values obtained on the whole Bathonian platform from 20 wells (environments calibrated with cores); Description of logging tools and units are available in Serra (1979)

Table 2b
Absolute depths against gamma ray log values for the shoreface to upper offshore domain

Gamma-ray A.P.I.	Depth (m)
0–15	20
16–30	30
31–45	40
46–55	50
56–65	60
66–75	70

(brachiopods association) that are found in relatively condensed intervals associated to marine flooding (Garcia and Dromart, 1997, Fig. 4).

3.2. Interval selection and final subdivision

Two conditions have to be met so that a stratigraphic surface (i.e. time-line) can be selected: (1) a confident physical correlation of the surface across the entire study area; (2) a reliable and accurate biostratigraphic assignment of it in order to have access to its geochronologic ages, so that the interval duration can be estimated.

Time-lines tie distinct depositional environments across the basin, and delineate packages of rocks whose thickness and composition vary as a function of their geographic location. Four time-lines have been selected for our calculation (Table 3). The choice of this spacing is a compromise between a time resolution as fine as possible and uncertainties (associated with the stratigraphic correlations and the interval durations) that raise with the resolution. The studied stratigraphic interval represents the lower half of the carbonate platform and encompasses the

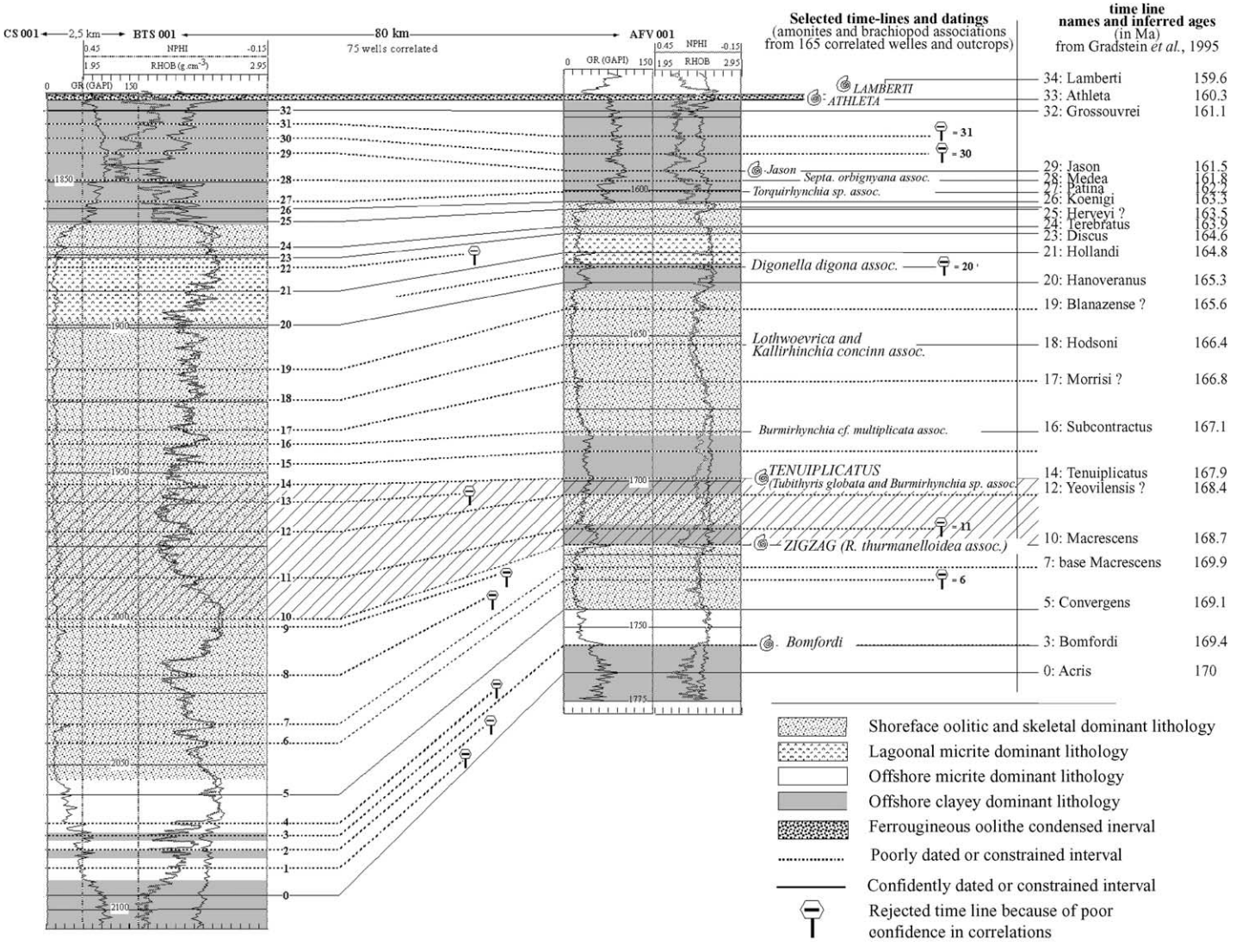

Fig. 3. Example of the method of correlation. The well log response is calibrated on outcrops located near the wells to determine the environment. The interval of study is between 169.1 and 167.1 Ma.

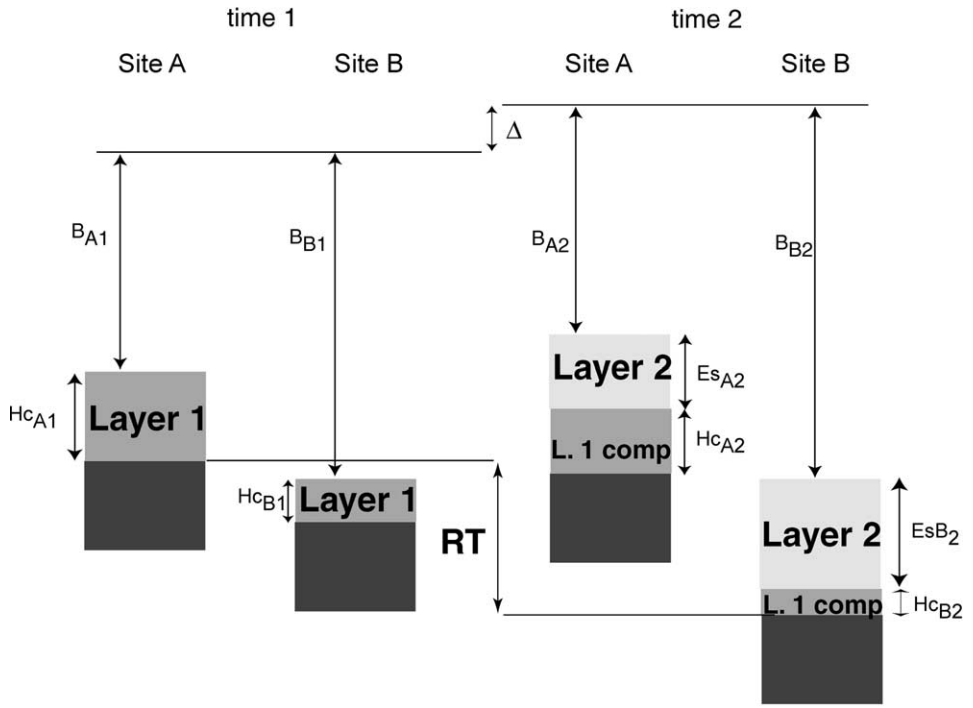

Fig. 4. Principle of calculation of relative tectonics (RT). See description of the equation in the text.

Table 3
Age of the selected time lines

	Markers (Fig. 2)	Age (Ma)
Line 4	M16	167.1
Line 3	M14	167.9
Line 2	M10	168.7
Line 1	M5	169.1

Lower to Middle Bathonian boundary. The interval shows the transition between the progradational pattern (lateral accretion) to the dominant aggradational pattern (vertical stacking) of strata that corresponds to the highest accumulation rates of carbonate sediments (Dromart et al., 2002).

3.3. Lithologies

The Bathonian of the Paris Basin is made up of a variety of limestone and shale lithologies associated with a large spectrum of depositional environments ranging from marginal marine to offshore domains. For instance, restricted marine depositional facies of the Lower/Middle Bathonian boundary (MD 14–MD 16 interval) are dominantly composed of a light-colored, chalky to massive peloidal micrite bearing large oncoids. Shoreface deposits (i.e., above the fair weather

wave base) are massive, coarse-grained limestone made up of grain-supported oolites and bioclasts (bivalves, gastropods, and coral debris). Storm-influenced deposits of the offshore zone correspond to a bioturbated, clayey, fine-grained limestones with bioclastic layers.

3.4. Depositional water depths

In the following, paleo-water depths have to be estimated at each site for each stratigraphic line to calculate the accommodation potential which is the space created for sediment to fill. The subdivision of paleo-depositional environments in terms of depths is based on the recognition of marine hydrodynamic limits. For an open carbonate shelf, three zones can theoretically be distinguished: the shoreface, above the fair weather (i.e., permanent) wave base; (2) the upper offshore, between the fair weather wave base and the storm weather wave base; (3) the lower offshore, below the storm wave base. The shoreface is characterized by the absence of fine-grained (i.e., clay-sized) sediments, because of the permanent re-suspension by waves. The upper offshore is marked by heterolitic facies, as an alternation of grainy, storm-related and fine-grained, suspension-derived deposits. The lower offshore theoretically show purely suspension-derived sediments. On wave-dominated shelves, a finer distinction is possible across the upper offshore from the morphology of storm current related erosive marks (Guillocheau, 1991).

Two domains (inner; middle-outer) have been discerned within the upper offshore of the Middle Jurassic in the Paris Basin from the observation of cores and exposed sections (Gaumet, 1997). Since the biotic assemblages and the primary sedimentary structures used can be seen on rocks only, a conversion of the well-log responses into depositional environments was realized through a set of 20 wells by directly comparing cores and well-log data (Table 2). It should be noticed that a depositional environment cannot be detected from the inspection of any single well-log but derives from the combination of well-log responses.

Eventually, an absolute water-depth value has been assigned to each domain (Table 2). In modern oceans, the depth of those hydrodynamic limits are variable. The lowermost boundary of the shoreface attains 30 m. Commonly, the limit between the middle and the outer upper offshore is 80 m and the depth of the storm wave base is about 130 m (Guillocheau, 1991). However, these values have been reduced for the study interval (1) because isotope paleobathymetry applied to the Middle Jurassic of the Paris Basin (Garcia et al., submitted) suggests a storm wave base around 110 m below the sea-level, (2) the general shallowing of the hydrodynamic limits associated with weaker storms is possibly related to the marginal position of the basin relative the open ocean that was the Tethys, and (3) because of the physiography itself of the basin (see Ziegler, 1988).

In the study interval, depositional environments include the shoreface and the upper offshore only. This domain has been divided into a number of sub-environments (six instead of three; Table 2b), in order : (1) to obtain a sufficient accuracy in estimating change of depositional water-depth between two successive time-lines at a given place and topographic gradients across the basin at a given time; (2) to make the acquisition of paleobathymetric data (656 values) reproducible and convenient. This extra-subdivision derives from an interpolation based on the double assumption that the gamma-ray log deflection is proportional to the clay content, and that the clay content itself varies linearly with the depositional water depth. In this respect, it should be noticed that shaley levels of the study interval do not contain any constituent prone to modify the

gamma-ray log response (i.e., phosphates and organic matter), and that it has already been shown that in general gamma-ray log values increase as depositional water-depth increase (Table 2). The water-depth allocation to each subenvironment represents a somewhat arbitrary interpolation based however on fairly reliable control points (e.g., storm wave base water depth). The error for water-depth estimates associated with the use of this subdivision is ± 5 m.

3.5. Uncertainties

The prominent uncertainty is associated with the calculation of rates because of the moderate control we have upon duration of chronostratigraphic intervals inferred through geochronologic scales. The time scale of Gradstein et al., (1994) is applied here because it incorporates new U/Pb and Ar/Ar dates, it tentatively erases the systematic discrepancy observed between low- and high-temperatures dates, and it is referred to the recent Mesozoic ammonite zonation. However, interpolation techniques used in constructing the total Jurassic time-scale are based on the assumption that ammonite subzones have equal duration. This is likely incorrect but the number of accurate and reliable tie-points in the Jurassic is still limited so that the standard deviation of an ammonite subzone duration, and the recurrence-time of brachiopod marker-beds (Garcia and Dromart, 1997), cannot be estimated. For the moment we have no real means of delineating errors associated with this interpolation and the resulting uncertainty tied to the calculation of rates might be up to 50%.

Finally, it should be noticed that even if we are concerned with fairly short time interval (i.e. less than half a million years), cyclostratigraphic dating has been rejected because of the following pitfalls : (1) a very large uncertainty is associated with recognition and hierarchy of stratigraphic cycles in shallow carbonate deposits because of common sedimentologic amalgamation; (2) an assignment of a given order of cycle (e.g., highest order) to a certain frequency of the Milankovitch band is somewhat arbitrary because of the large fluctuation of accumulation rates in a given site—an effect of spatial volumetric partitioning of sediments and cycle superimposition (Dromart et al., 1996); (3) the fact that the duration of carbonate elementary cycles can definitely be out of the Milankovitch frequency band (Brack et al., 1996).

3.6. Compaction corrections

The thickness of each layer at time of deposition has been calculated using a decompaction procedure similar to those proposed by Angevine et al. (1990). The compaction is assumed to be related to a change in porosity which depends on burial depth. A simple exponential relationship connecting change in porosity with depth has been applied (Angevine et al., 1990). The parameters of this relation are a function of the lithology (Table 4). A maximum burial depth has been estimated to 1500 m for each well (Guillocheau et al., 2000). This depth is the maximum thickness of the sedimentary pile above the considered interval. The value of this thickness has not to be accurate since the maximum compaction occurs through the upper 500 m of burial (Angevine et al., 1990). The sedimentary thickness of the layer located under the study interval has been assumed to be 500 m, which is the maximum thickness of the sedimentary pile under the study interval (Guillocheau et al., 2000). This basal layer has been considered as homogeneous and made up of a lithology with parameters intermediate between shale and carbonates in order to

represent in average the behavior of this layer. The basement under the Triassic layer is considered as not compactable. With the chosen parameters, the calculated thickness of deposits is a maximum value as no early cementation has been considered. So the carbonate sedimentation rates are possibly overestimated. However, even in this case, the spatial gradients of sedimentation are conserved and the overall geometry is preserved because the more compactable clayey layers are much thinner than the limestone levels.

4. Relative tectonics

A signal of vertical displacement has been extracted from bathymetric data and from the thickness of the sedimentary layers according to a method described by Dromart et al. (1998). The absolute vertical displacement (T_A) of a point located in the basement under the sedimentary layer submitted to compaction is (Fig. 4):

$$T_A = (Hc_{A2} + Es_{A2} + B_{A2} + \Delta) - (B_{A1} + Hc_{A1}) \quad (2)$$

with, Hc_{A1} is the thickness of the sedimentary layer deposited before time 1 at the point A, Hc_{A2} is the thickness of the sedimentary layer deposited before time 1 and compacted between time 1 and time 2, B_{A1} (B_{A2}) is the water depth at the point A at the time 1 (time 2), Es_{A2} is the thickness of the sedimentary layer deposited at point A between times 1 and 2, and Δ is the eustatic variation between time 1 and time 2. There is no agreement on a chart of eustatic variation at time steps shorter than 1 My for Jurassic time (Hallam, 2001), making the eustatic parameter Δ impossible to estimate. However, since eustasy is uniform in space by definition, the vertical displacement of a point can be measured relatively to a reference point for which the same calculation is done. The relative vertical displacement that we call "Relative Tectonics" (RT) is equal to the difference between the two absolute displacements (Fig. 4):

$$\begin{aligned} Tr &= T_A - T_B \\ &= (Hc_{A2} - Hc_{A1}) + (B_{A2} - B_{A1})Es_{A2} - (Hc_{B2} - Hc_{B1}) - (B_{B2} + B_{B1}) - Es_{B2} \end{aligned} \quad (3)$$

The eustatic variation cancels out in this formula. RT has been calculated for each well of the Paris basin and for each time step taking a reference point in the center of the basin. The value of the relative tectonics for a given well has no meaning as this value depends on the reference point. Only spatial gradients of relative tectonics are indicative of the relative vertical displacement between the points. If a homogeneous tectonic component exists on a larger scale than the area of study, it is not detected by this method as it is included in the "eustatic" part of the signal.

Table 4
Parameters of decompaction from Angevine et al. (1990) for lithologies of the Paris Basin during Dogger[a].

	Shale	Limestone
Surface porosity (Φ_0)	0.5	0.5
Exponential factor (N, m^{-1})	0.0005	0.0007

[a] The relation between porosity and depth is: $\Phi = \Phi_0 \exp(-Nz)$ with Φ_0 porosity at the surface and z depth of burial.

The values of RT and of the thickness of decompacted sedimentary layer divided by the time steps have been linearly interpolated to obtain maps of RT velocity and sedimentation velocity. Water depth and water depth variations between two time lines have been interpolated by the method of nearest neighbor. On the period of time between 169.1 and 168.7 Ma, the amplitude of *RT* is 90 m (Fig. 5). The spatial variation of RT is low in the eastern part of the Paris basin. The western part is affected by higher spatial gradients of RT. The position of the highest gradient is related to the activity of the Seine fault (Fig. 2). During this period, the sedimentation rate ranges from 0 to 100 m My^{-1}. The sedimentation rate is higher in the eastern side than in the western side where the major faults are active. The water depth map shows that the eastern part of the Paris basin is a shallow water platform whereas water depths in the western part are more variable. The Paris basin has the same behavior during the two following periods (Figs. 6 and 7). The eastern part of the basin remains a shallow water platform with a sedimentation rate around 50–80 m My^{-1}. The sedimentation rate is lower and depths more variable in the western side. The platform domain is always affected by a diffuse RT with depths varying in a limited range between two time surfaces. On each map of RT, patches of diffuse downward RT located on the platforms are correlated with high sedimentation rates. The gradient of RT between the center and the border of the patches is equal to the difference of sedimentation rates (i.e., $\sim$30 m My^{-1}). The surface of the patches is around 400 km^2 with a radius of about 10 km. The location of the patches evolved with time on the carbonate platform. Even if the water depth remained constant, the major accumulation of sediment moved toward the west.

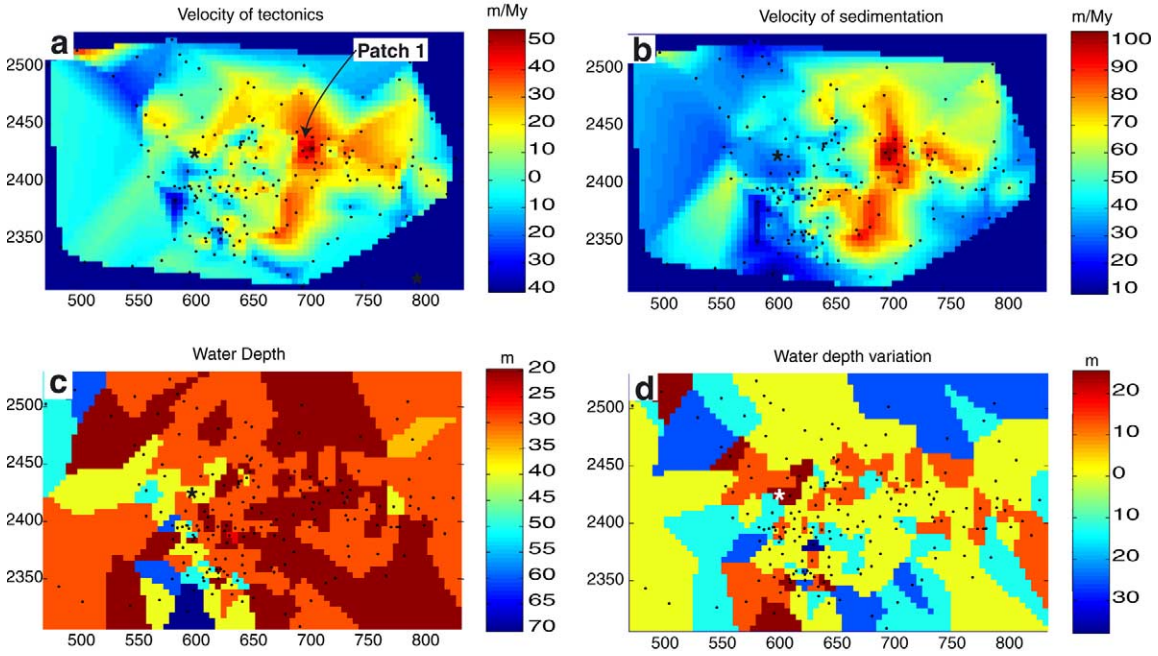

Fig. 5. Map of (a) RT, (b) sedimentation velocity, (c) water depth (d) change of water depth for the period between 169.1 and 168.7 Ma. Notice the correlation of the strong gradients of RT with the major faults of the Paris Basin (Seine and Bray faults, Fig. 2) and the region of diffuse RT correlated with high sedimentation rate on the eastern part of the Paris Basin. The stars indicate the position of Paris.

5. Model of subsidence of sedimentary bodies

Two different tectonic behaviors are visible on RT maps: (1) a localized subsidence which is not correlated with the sedimentation rate and (2) a diffuse subsidence affecting the platform domains and correlated with high sedimentation rate. The first behavior is observed along the major faults of the Paris basin. This classical tectonic activity is generated by strain and stress applied at boundaries of the basin. It will be demonstrated in the following that the second kind of subsidence could be associated with the in situ growth of carbonate platforms.

A simple 2D numerical model has been developed based on the model of mantle relaxation after the melting of an ice cap (e.g. Turcotte and Schubert, 1982) in order to test whether spatial and temporal length scales of construction and subsidence of sedimentary bodies are consistent with realistic values of viscosity for the lower crust. The topography of the sedimentary body is considered as infinite, sinusoidal, and at steady state (Fig. 8). Topography is maintained by sedimentation and is absorbed by the flow of a viscous channel composed by the lower crust or a part of it. The uplift generated away from the load by the flow of the crust is neglected. The mantle is considered as rigid for such low wavelength load and thus non reactive. The elastic part of the crust is neglected. The rheology of crustal rocks is considered as viscous newtonian. The equations which govern this process with the boundary conditions described in Fig. 7 are given in

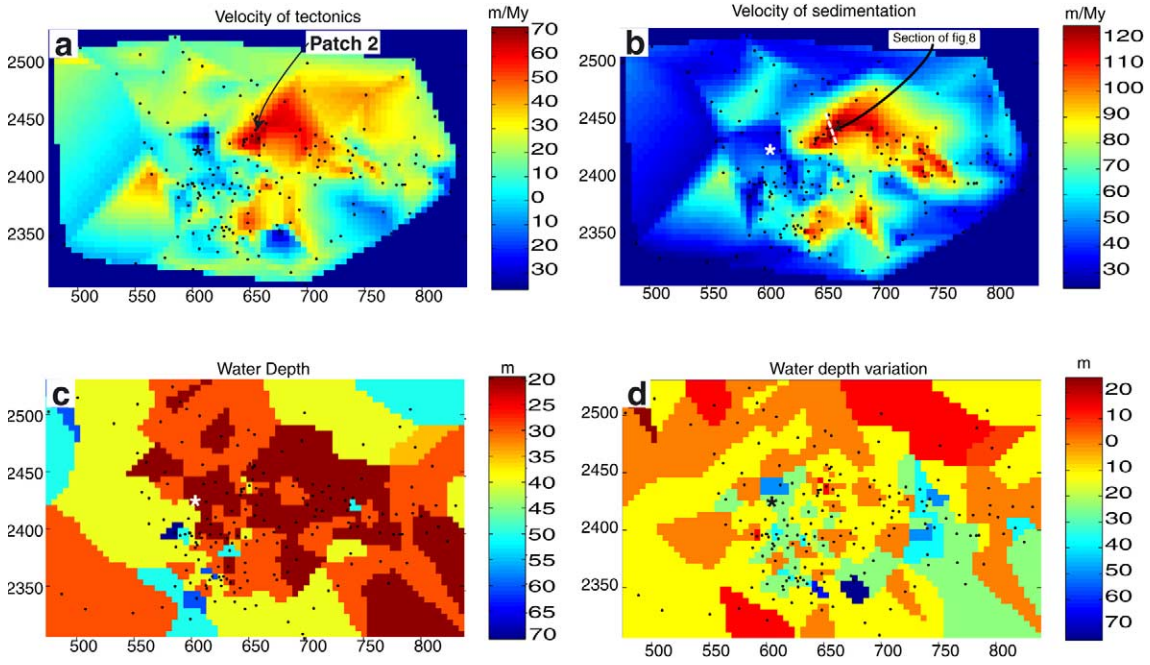

Fig. 6. Map of (a) RT, (b) sedimentation velocity, (c) water depth, (d) change of water depth for the period between 168.7 and 167.9 Ma. Notice that the patch of downward diffuse RT located on the eastern part of the basin has moved toward the west. The water depth on the platform is the same as the water depth of the previous period. The white dashed line shows the position of the section presented in Fig. 9. The stars indicate the position of Paris.

the Appendix. It is assumed that the system rapidly reaches steady state. This assumption is consistent with the fact that the thickness of the bioclastic piles are at least two times the water depth under which they have been deposited and that the water depth remains constant throughout the study interval (Figs. 5–7). The other strong assumption of the subsidence model of sedimentary bodies is that the patches have a positive topography of 5–10 m above the surrounding platform. Even if such an elevation contrast cannot be directly and precisely measured, topographic gradients can be qualitatively estimated through well-log data observation. Fig. 9 shows well-logs of a north–south section across a patch located in the center of the Paris basin from 168.7 to 167.9 Ma (Fig. 6). The sedimentary thickness increases from the north to the middle of the section and decreases toward the south. In the middle of the section, the Gamma Ray (GR) signal displays a blocky pattern typical of a carbonate shoal. The GR signal becomes noisier towards the section extremities reflecting the occurrence of a higher number of clay rich layers. Therefore, environments at the toes of the depositional profile were certainly closer to the hydrodynamic threshold that is the Shoreface–Offshore limit (i.e., possible clay-sized deposition). The sensitivity of the lithologic record to minor sea level variations (i.e., fourth and fifth orders rapid and small amplitude variations resulting from climatic cycles) was higher at the extremities of the carbonate body. It can be definitively concluded that the depth of the carbonate patches was lower in the center of the structure than on the edges.

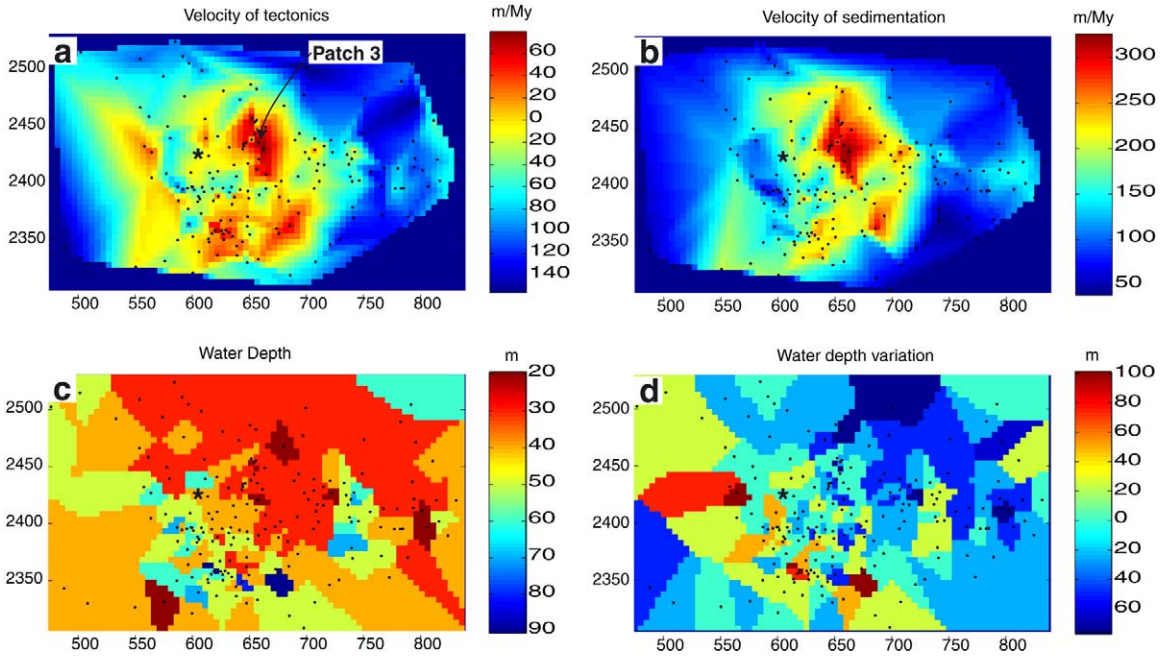

Fig. 7. Map of (a) RT, (b) sedimentation velocity, (c) water depth, (d) change of water depth for the period between 167.9 and 167.1 Ma. The patch of downward diffuse RT is in the center of the basin. The difference in the sedimentation rate between the center and the border of the patch is equal to 20 m My^{-1}. The stars indicate the position of Paris.

The variation of the topography of the bioclastic pile above the surrounding platform is given in 1D by the relation:

$$\frac{\mathrm{d}E}{\mathrm{d}t} = Vs - Vf \tag{4}$$

where Vs is the difference between the sedimentation velocity over the bioclastic patch and the sedimentation velocity over the surrounding platform, and Vf is the velocity of vertical flow in the crust under the load. Vf is proportional to with the topography at a time t [$E(t)$] and to the inverse of the viscosity ($1/\eta$) (see Appendix) (Lliboutry, 1976):

$$Vf(t) = \alpha \frac{E(t)}{\eta} \tag{5}$$

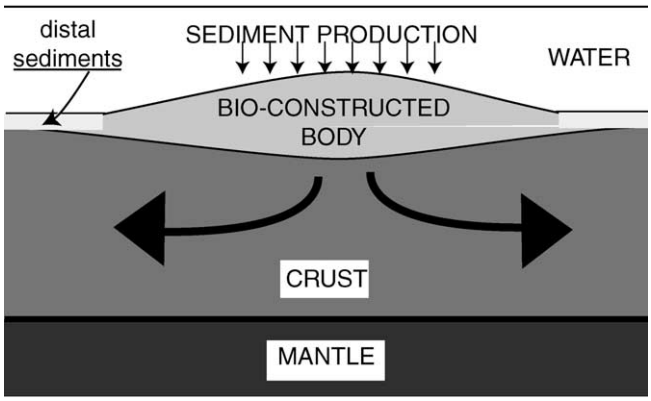

Fig. 8. 2D model of subsidence below the carbonate patches. The top of the patch is assumed to be located from 5 to 10 m above the rest of the platform. The load produced by this elevation induces a flow in the lower crust which tends to reduce the elevation. The elevation is maintained by in situ construction of bioclastic carbonate.

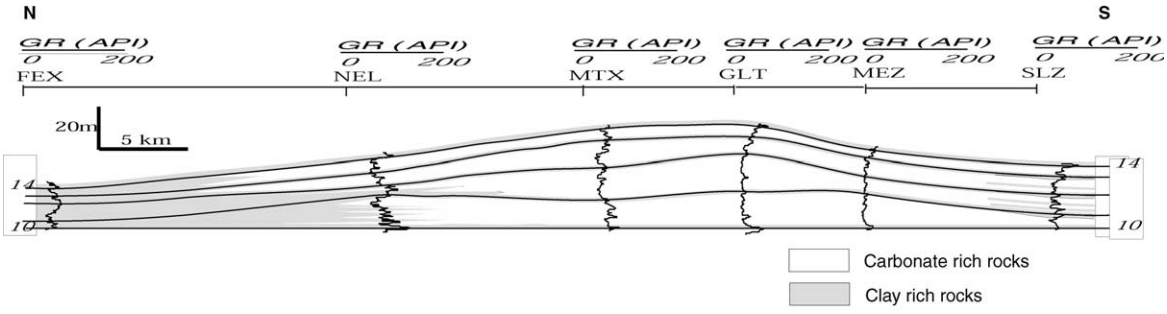

Fig. 9. Correlation of the well logs for the well on the section shown in Fig. 6. Carbonate rocks are more abundant where the thickness is larger indicating that the water depth was lower in this region. (FEX, Feigneux well; NEL, Neufchelles well; MTX, Monthieux well; GLT, Glairet well; MEZ, Melarchez well; SLZ, Champotran well).

where α is a function of the thickness of the channel, of the wave length of the sedimentary body, and of the density contrast between the sediment and the flowing lower crust. At steady state, Vs is equal to Vf. Then, the ratio of Vs and E is constant and depends on the thickness and viscosity of the flowing lower crust for a given wavelength:

$$\frac{Vs}{E} = \frac{\alpha}{\eta} \tag{6}$$

The values of Vs/E at steady state are reported in Fig. 10 for wave-lengths of sedimentary bodies ranging from 20 to 100 km, viscosity of the lower crust ranging from 10^{19} to 10^{21} Pa s, and thickness of the crustal channel ranging from 7 to 15 km. Due to the lack of precision of the measured topography, two values of Vs/E are considered: one for a topography of 10 m and one for a topography of 5 m. The measured values of Vs/E have been reported also on Fig. 10 with uncertainty of 2 times the measured value of Vs. The characteristics of the bioclastic patches are located close to the 10^{21} Pa s curves and for small thickness of the crustal channel. This value of viscosity is 2 orders of magnitude higher than the value generally inferred from other contexts

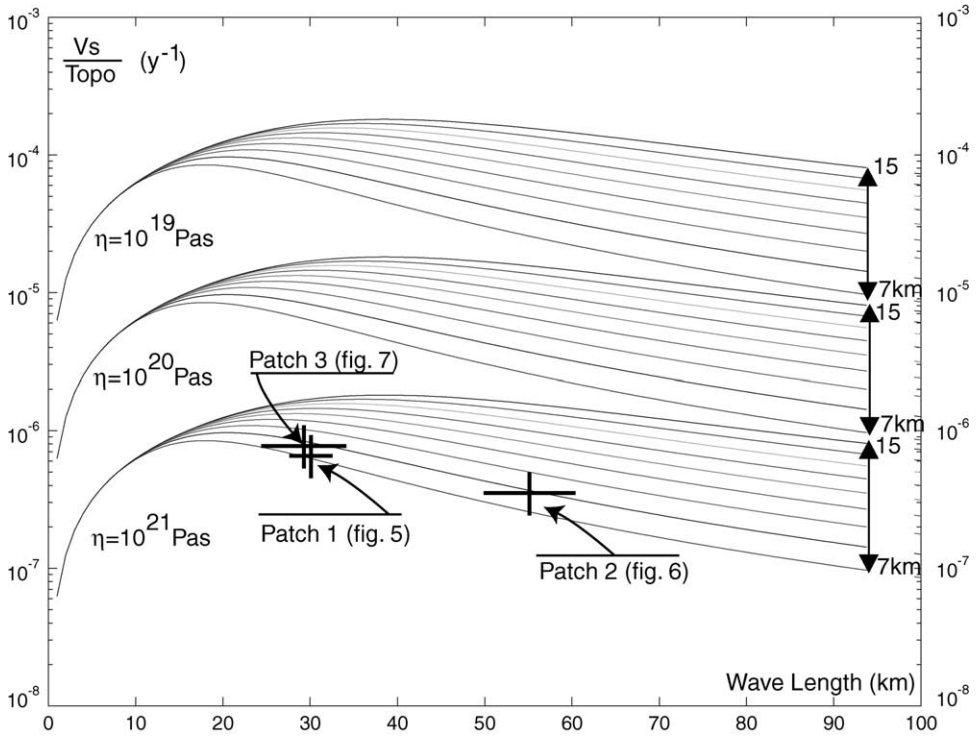

Fig. 10. Load wavelength vs. Vs/E ratio for viscosity of the crust of 10^{19}–10^{21} Pa s and thickness of the flowing crust of 7–15 km. The velocities of sedimentation have been measured for each patch marked in Figs. 5–7. The ratio Vs/E has been calculated for each patch assuming a topography between 5 and 10 m. The values of Vs/E are reprted vs. the width of the patches.

such as the Basin and Range province (Kruse et al., 1991). It should be noted that the viscosity is sensitive to the load and to the temperature (e.g. Ranalli, 1997) via the formula (see Table 1 for explanation of the symbols):

$$\eta = M^{-1}\sigma^{1-n}e^{(Q/RT)} \tag{7}$$

As the basin and Range province has undergone a large and recent tectonic activity, the average temperature of the crust is higher than the geotherm under the Paris basin during the Middle Jurassic. For an activation energy (Q) of 200 kJ mol^{-1}, which is the average activation energy of crustal rocks (Ranalli, 1997), an increase of temperature from 550 to 650 reduces the viscosity by a factor of 20. As rocks follow non-newtonian rheology, the viscosity depends also on the load and decreases with it. The loads in the Paris basin are generated by topographic differences of 5–10 m. Their order of magnitude is 10^5 Pa. In the Basin and Range province the loads studied by Kruse et al. (1991) are exerted by topographic differences of 100 m and are thus 10 times higher. For a stress exponent (n) of 3, an increase of the load from 10^5 to 10^6 Pa reduces the viscosity by a factor of 100. The combination of thermal and load effects can thus explain the difference of viscosity calculated in the Paris basin and in the Basin and Range province. The value of viscosity found here falls in the range of viscosities estimated by Al-Zoubi and ten Brinck (2002) for lower crust in a non-perturbed heat flow region.

Pressure solution creep which is a mechanism active in the upper part of the crust, could be also a possible mechanism of flow responsible of the subsidence of the bioclastic sedimentary bodies of the Paris basin. The viscosity associated with this mechanism is around 10^{21} Pa s (Gratier et al., 1999), similar to the viscosity measured in the present study. Pressure solution creep is active in both sedimentary and metamorphic rocks containing either carbonates or quartz and thus could be active in the basement of the Paris basin composed mainly by Hercynian metamorphosed rocks (Guillocheau et al., 2000).

The thickness of the flowing crust is also a parameter which can be extracted from the model. The thickness falls in the range between 7 and 10 km. However, this thickness is very sensitive to small changes of the viscosity and cannot be meaningfully discussed.

6. Discussion

6.1. Limits of the model

The model described above has some limitations relative to what is known concerning the rheology and densities of the lithosphere and relative to the process of subsidence itself.

The rheology of the lithosphere has been simplified. The elastic part of the crust has been neglected because other studies (Garcia-Castellanos et al., 2000; Le Solleuz et al., submitted) show that the thickness of the equivalent elastic layer of the crust is less than 10 km thick under the Paris basin and adjacent regions. The inclusion of elasticity in the model would produce a decrease of the value of the viscosity because the elastic layer would slow down the subsidence process. We use a newtonian law of viscosity for rocks. The rheology of the lithosphere is more complex as rocks can be brittle, plastic, elastic and viscous. However, the newtonian approach has been validated by Kruse et al. (1991) by comparison between velocity distribution in

newtonian and power law channelized flow. The lithospheric mantle has been considered as non reactive. Finite elements calculations (Wdowinsky and Axen, 1992) have shown that even with loads larger than those studied here and for mantle viscosity equal to 100 times the lower crust viscosity, the maximum velocity of flow in the mantle is hundred times lower than the velocity in the lower crust.

Concerning the process of subsidence, the flow has been considered to be 2D rather 3D. The patches are generally elongated in the north south direction and their shape is rather elliptic than circular. Then the main flow will occur perpendicular to the patches elongation and can be thus considered approximately as two dimensional. We have neglected the uplift of the floor produced by the flow away from the patches. We have considered the load at steady state whereas it increases in width with time. The equations of subsidence derived in the Appendix and Fig. 10 show that for the considered range of viscosity, the velocity of subsidence is not very sensitive to the width of the load. If the width of the load increases from 40 to 80 km for a viscosity of 10^{20} Pa s and a thickness of the flowing channel of 20 km, the velocity of subsidence decreases from 8 10^{-11} to 6 10^{-11} m s^{-1}. Thus, this effect is negligible relative to the effect of viscosity.

6.2. Subsidence

It is obvious that the whole subsidence observed in the Paris basin is not produced by the flow of the crust under the sedimentary load. An external tectonic mechanism is necessary to initiate the creation of accommodation space. Two kinds of models have been proposed in literature, one based on successive limited phases of extension, and one based on the thermal relaxation of the lithosphere after an extension phase.

In the first model, the Paris basin has been submitted to several limited extensive phases which have created the accommodation space (e.g. Loup and Wildi, 1994). It has been demonstrated (Guillocheau, 1991), that the tectonic extensive phases which occur at the limit of the European plates are recorded in the Paris basin. The opening of the Atlantic Ocean, the North-Sea, and Tethys ocean are synchronous with some accelerations of subsidence (Robin et al., 2000). For the second model, the long duration of the subsidence implies a strong initial thermal anomaly and thus a large amount of extension (e.g. Prijac et al., 2000). For the Paris basin, subsidence data are compatible with an initial value of Mckenzie (1978) β parameter ranging from 1.39 to 1.46, and of 1.27 if a 40 km thick lithospheric root has detached (Brunet and Le Pichon, 1982). The extension phase was possibly between Carboniferous to middle Permian. The general shape of the accommodation curve fits a thermal relaxation model as subsidence rate decreases exponentially with time (Robin et al., 1996). In such context, the tectonics generated by bioconstruction would be superimposed on a long wave length signal of thermal origin.

7. Conclusion

Vertical relative displacement can be measured in sedimentary basins from water depth and sedimentary thickness at a time resolution shorter than 1 My by tracking identifiable stratigraphic surfaces. Applied to the Paris basin during the Bathonian, this technique shows that the basin can be divided into two distinct depositional domains: a western area with water-depth exceeding 60

m, slow sedimentation and bathymetry controlled by some major faults, and a eastern domain with shallow water, enhanced carbonate accumulation, and low topographic gradients. Over this last domain, carbonate bioclastic patches of 50 km axis and 10–40 m in thickness were accumulated under a steady bathymetry trough time. The spatial and kinematic characteristics of these patches suggest that the subsidence beneath the patches was related to the flow of the lower crust under the load produced by sediments. The viscosity of the lower crust would be around 10^{21} Pa s, a value compatible with the thermal and mechanical state of the crust.

Acknowledgements

M.P. Doin and R. Stephenson are thanked for their constructive reviews and helpful comments. N. Coltice is thanked for comments on a previous version of the paper. This work has been supported by INSU IT program "Comportement dynamique des plateformes carbonatées".

Appendix. Solution of the equations of velocity

The velocity field is computed from the general biharmonic equation of the stream function. The general solution of the stream function for periodic boundary conditions is (e.g. Fleitout and Froidevaux, 1982; Turcotte and Schubert, 1982):

$$\psi = \sin\tfrac{2\pi x}{\lambda}(Ae^{-2\pi y/\lambda} + Bye^{-2\pi y/\lambda} + Ce^{2\pi y/\lambda} + Dye^{2\pi y/\lambda}) \tag{A1}$$

The vertical (v) and horizontal (u) components of velocity are then:

$$\begin{aligned} u(x, y, \lambda, H) &= -\tfrac{\partial\psi}{\partial y} \\ &= \sin\frac{2\pi x}{\lambda}[e^{-2\pi y/\lambda}(\frac{2\pi}{\lambda}A + \frac{2\pi}{\lambda}By - B) + e^{2\pi y/\lambda}(-\frac{2\pi}{\lambda}C - \frac{2\pi}{\lambda}Dy - D)] \end{aligned} \tag{A2}$$

$$v(x, y, \lambda, H) = \tfrac{\partial\psi}{\partial x} = \frac{2\pi}{\lambda}\cos\frac{2\pi x}{\lambda}[e^{-2\pi y/\lambda}(A + By) + e^{2\pi y/\lambda}(C + Dy)]$$

The pressure can be computed from the horizontal force balance (e.g. Turcotte and Schubert, 1982):

$$\eta\left(\frac{\partial^2 u}{\partial x^2} + \frac{\partial^2 u}{\partial y^2}\right) - \frac{\partial p}{\partial x} = 0 \tag{A3}$$

Replacing u by its value, Eq. (A3) can be integrated for pressure:

$$p(x, y, \lambda, H) = -4\eta\cos\frac{2\pi x}{\lambda}e^{2\pi y/\lambda}\left(Be^{-4\pi y/\lambda} + D\right) \tag{A4}$$

For the problem of subsidence of sedimentary bodies in a ductile crust, the boundary conditions are:

no horizontal velocity at the surface (surface rigid crust) $Uf(x, 0, \lambda, H = 0)$ (A5)

no velocity at the Moho (rigid mantle): $Vf(x, H, \lambda, H) = 0$ (A6)

and $Uf(x, H, \lambda, H) = 0$ (A7)

load applied at the surface: $q(x) = (\rho_c - \rho_w)gE \sin\frac{2\pi}{\lambda}x$ (A8)

Because vertical surface displacement is small relative to crust thickness, the pressure at the surface ($y = 0$) is equal to the load produced by the sedimentary body which has a sinusoidal shape:

$$p(x, 0, \lambda, H) = q(0)\sin\frac{2\pi x}{\lambda} \tag{A9}$$

Equation for the unknowns A, B, C, and D can be extracted from the boundary conditions:

$$\begin{pmatrix} k & -1 & -k & -1 \\ \frac{k}{l} & \frac{kH}{l} - \frac{1}{l} & -lk & -l(1+kH) \\ \frac{1}{l} & \frac{H}{l} & l & Hl \\ 0 & 1 & 0 & 1 \end{pmatrix} \begin{pmatrix} A \\ B \\ C \\ D \end{pmatrix} = \begin{pmatrix} 0 \\ 0 \\ 0 \\ \frac{q0}{2k\eta} \end{pmatrix} \tag{A10}$$

where k is the wave number and $1 = e^{kH}$. The linear system is solved symbolically with Mapple and numerically with Matlab for various values of k, H, $q0$, η. The numerical values of the unknowns are then replaced in Eqs. (A2).

In the system considered here, the velocity is at steady state. The maximum vertical velocity at the surface which is reached at $x = 0$ is:

$$Vf(0, 0, \lambda, H) = \frac{2\pi}{\lambda}(A + C) \tag{A11}$$

Replacing A and C by their values:

$$Vf(0, 0, \lambda, H) = -\frac{1}{2}\frac{-l^4 + 4H^2k^2l^2 + 2l^2 - 1}{k(4l^2kH + l^4 - 1)}\frac{(\rho_c - \rho_w)gE}{\eta} \tag{A12}$$

The parameter α of the Eq. (5) is then:

$$\alpha = -\frac{1}{2}\rho g\frac{-l^4 + 4H^2k^2l^2 + 2l^2 - 1}{k(4l^2kH + l^4 - 1)} \tag{A13}$$

References

Al-Zoubi, A., ten Brink, U., 2002. Lower crustal flow and the role of shear in basin subsidence: an example from the Dead Sea basin. Earth Planet. Sci. Lett. 199, 67–79.

Angevine, C.L., Heller, P.L., Paola, C., 1990. Quantitative sedimentary basin modeling. American Association of Petroleum Geologists, Continuing Education Course Note Series 32

Avouac, J.P., Burov, E.B., 1996. Erosion as a driving mechanism of intracontinental mountain growth. J. Geophys. Res. 101, 17747–17769.

Bills, B.G., Currey, D.R., Marshall, G.A., 1994. Viscosity estimates for the crust and upper mantle from patterns of lacustrine shoreline deformation in the Eastern Great Basin. J. Geophys. Res. 99, 22059–22086.

Brack, P., Mundil, R., Oberli, F., Meier, M., Rieber, H., 1996. Biostratigraphy and radiometric age data question the Milankovitch characteristics of the Latemar cycles (Southern Alps, Italy). Geology 24 (4), 371–375.

Brunet, M.F., Le Pichon, X., 1982. Subsidence of the Paris basin. J. Geophys. Res. 87, 8547–8560.

Bott, M.P.H., 1999. Modeling local crustal isostasy caused by ductile flow in the lower crust. Jour. Geophys. Res. 104 (B9), 20349–20359.

Buck, W.R., 1991. Modes of continental lithospheric extension. J. Geophys. Res. 96 (B12), 20161–20178.

Burov, G., Cloetingh, S., 1997. Erosion and rift dynamics: new thermomechanical aspects of post-rift evolution of extensional basins. Earth Planet. Sci. Lett. 150, 7–26.

Deng, J., Gurnis, M., Kanamori, H., Hauksson, E., 1998. Viscoelastic flow in the lower crust after the 1992 Landers, California, Earthquake. Science 282, 1689–1692.

Dromart, G., Ader, M., Allemand, P., Curial, A., Guillocheau, F., Vidal, G., 1996. Delineation of hybrid and carbonate reservoirs through genetic stratigraphy in the Lower Mesozoic of the western Subalpine basin, SE France: Procedures and Benefits. Marine and Petroleum Geology 13 (6), 654–670.

Dromart, G., Allemand, P., Quiquerez, A., 1998. Calculating rates of syndepositional normal faulting in the western margin of the Mesozoic subalpine basin (south-east France). Basin Research 10, 235–260.

Dromart, G., Garcia, J.P., Allemand, P., Gaumet, F., Rousselle, B., 2002. A volume-based calculation of carbonate accumulation in the middle Jurassic of France. J. Geol. 110–112, 195–210.

Fleitout, L., Froidevaux, C., 1982. Tectonics and topography for a lithosphere containing densiy heterogeneities. Tectonics 1 (1), 21–56.

Garcia, J.P., Dromart, G., Guillocheau, F., Allemand, P., Gaumet, F., Robin, C., Sambet, G., 1996. Bathonian-Callovian Paris Basin—Subalpine Basin intercorrelations along an Ardennes-Ardèche cross-section. C.R. Acad. Sci. Paris 323 (IIa), 697–703.

Garcia, J.P., Dromart, G., 1997. The validity of two biostratigraphic approaches in sequence stratigraphic correlations: brachiopod zones and marker beds in the Jurassic. Sedimentary Geology 114, 55–79.

Garcia J.P., Sheppard, S., Lecuyer, C., Picard, S. Carbon and oxygen isotope composition of Jurassic brachiopods: paleoenvironmental reconstructions of tropical carbonate depositional settings. Earth Planet Sci Lett. Submitted for publication.

Garcia-Castellanos, D.S., Cloetingh, S., Van Balen, R., 2000. Modelling the middle pleistocene uplift in the Ardennes-Rhenish massif: thermomechanical weakening under the Eifel? Global and Planetary Change 27, 39–52.

Gaumet, F., 1997. Fondements géologiques pour la modélisation stratigraphique des sytèmes carbonatés: Le Jurassique moyen de l'Angleterre à la Méditerranée. Unpublished PhD Thesis, University of Lyon, France.

Gradstein, F.M., Agterberg, F.P., Ogg, J.G., Hardenbold, J., Veen Van, P., Thierry, J., Huang, Z., 1994. A Mesozoic time scale. J. Geophys. Res. 99 (B12), 24051–24074.

Gratier, J.P., Renard, F., Labaume, P., 1999. How pressure solution creep and fracturing processes interact in the upper crust to make it behave in both brittle and viscous manner. J. Struct. Geol. 21, 1189–1197.

Guillocheau, F., 1991. Modalités d'empilement des séquences génétiques dans un bassin de plate-forme (Dévonien armoricain): nature et distorsion des différents ordres de séquences de dépôts emboîtées. Bull. Centre Rech. Expl. Prod. Elf Aquitaine 15 (2), 383–410.

Guillocheau, F., Robin, C., Allemand, P., Bourquin, S., Brault, N., Dromart, G., Friedenberg, R., Garcia, J.P., Gaulier, J.M., Gaumet, P., Grosdoy, B., Hanot, F., Le-Strat, P., Mettraux, M., NalPa s, T., Prijac, C., Rigollet, C., Serrano, O., Grandjean, G., 2000. Meso-Cenozoic geodynamic evolution of the Paris Basin: 3D stratigraphic constraints. Geodinamica-Acta 13 (4), 189–245.

Hallam, A., 2001. A review of the broad pattern of Jurassic sea-level changes and their possible causes in the light of current knowledge. Palaeogeography, Palaeoclimatology, Palaeoecology 167, 23–37.
Hopper, J.R., Buck, W.R., 1996. The effect of lower crustal flow on continental extension and Passive-margin formation. J. Geophys. Res. 101 (B9), 20175–20194.
Kaufman, P.S., Royden, L.H., 1995. Lower crustal flow in an extensional setting: constraints from the Halloran Hills region, eastern Mojave desert, California. J. Geophys. Res. 99 (B8), 15,723–15,739.
Klein, A., Jacoby, W., Smilde, P., 1997. Mining-induced crustal deformation in Northwest Germany: modelling the rheological structure of the lithosphere. Earth Planet. Sci. Lett. 147, 107–123.
Klemann, V., Wolf, D., 1999. Implications of a ductile crustal layer for the deformation caused by the Fennoscandian ice sheet. Geophys. J. Int. 139, 216–226.
Kruse, S., MCNutt, M., Phipps-Morgan, J., Royden, L., 1991. Lithospheric extension near lake Mead, Nevada: a model for ductile flow in the lower crust. J. Geophys. Res. 96 (B3), 4435–4456.
Le Solleuz, A., Doin, M.-P., Robin, C., Guillocheau, F., 2003. From a mountain belt collapse to a sedimentary basin development: 2-D thermal model based on inversion of stratigraphic data in the Paris basin. Tectonophysics. Submitted for publication.
Lliboutry, L., 1976. Isostasie, propriétés rhéologiques du manteau supérieur. In: Coulomb, J., Jobert, M. (Eds.), Traité de Géophysique interne. Masson, p. 354.
Loup, B., Wildi, W., 1994. Subsidence analysis in the Paris basin: a key to Northwest European inracontinental basins? Basin Research 6 (2-3), 159–177.
MacCready, T., Snoke, A.W., Wright, J.E., Howard, K.A., 1997. Mid-crustal flow during tertiary extension in the Ruby mountain core complex, Nevada. Geol. Soc. Am. Bull. 109 (12), 1576–1594.
McKenzie, D., 1978. Some remarks on the development of sedimentary basins. Earth Planet. Sci. Lett. 40, 25–32.
McKenzie, D., Nimmo, F., Jackson, J.A., Gans, P.B., Miller, E.L., 2000. Characteristics and consequenses of flow in the lower crust. J. Geophys. Res. 105 (B5), 11029–11046.
McQuarrie, N., Rodgers, D.W., 1998. Subsidence of a volcanic basin by flexure and lower crustal flow: the eastern Snake River Plain, Idaho. Tectonics 17 (2), 203–220.
Pinet, B., Coletta, B., 1990. Probing into extensional sedimentary basins: comparison of recent data and derivation of tentative models. Tectonophysics 173, 185–197.
Prijac, C., Doin, M.P., Gaulier, J.M., Guillocheau, F., 2000. Subsidence of the Paris basin and its bearing on the late Variscan lihosphere evolution: a comparison between Plate and Chablis models. Tectonophysics 323, 1–38.
Ranalli, G., 1997. Rheology of the lithosphere in space and time. In: Burg, J.P., Ford, M. (Eds.), Orogeny through Time. Geol. Soc. London Spec. Publ., No. 121, pp. 19–37.
Ranalli, G., Murphy, D.C., 1987. Rheological stratification of the lithosphere. Tectonophysics 132, 281–295.
Robin, C., Guillocheau, F., Gaulier, J.M., 1996. Mesure des signaux eustatiques et tectoniques au sein de l'enregistrement sédimentaire d'un basin intracratonique. Application au Lias du Bassin de Paris. C.R. Acad. Sci. Paris, Ser. IIa 322, 1079–1086.
Robin, C., Guillocheau, F., Allemand, P., Bourquin, S., Dromart, G., Gaulier, J.M., Prijac, C., 2000. Echelles de temps et d'espace du contrôle tectonique d'un bassin flexural: le bassin de Paris. Bull Soc. Geol. France 171 (2), 81–196.
Rydelek, P.A., Sacks, I.S., 1990. Asthenospheric viscosity and stress diffusion: a mechanism to explain correlated earthquakes and surface deformation in NE Japan. Geophys. J. Int. 100, 39–58.
Serra, O., 1979. Diagraphies différées—bases de l'interprétation. Tome 1: acquisitions des données diagraphiques. Bull. Centre Rech. Expl. Prod. Elf-Aquitaine, Mém. 7.
Stel, H., Cloetingh, S., Heeremans, M., van der Beek, P., 1993. Anorogenic granite, magmatic underplating and the origin of intracratonic basins in a non-extensional setting. Tectonophysics 226, 285–299.
Turcotte, D., Schubert, G., 1982. Geodynamics: Applications of Continuum Physics to Geological Problems. John Wiley and Sons.
Underhill, J.R., Partington, M.A., 1993. Use of genetic sequence stratigraphy in defining and determining a regional tectonic control on the "Mid-Cimmerian unconformity"—implications for North-Sea Basin development and the global sea-level chart. In: Weimer, P., Posamentier, H.W. (Eds.), Siliciclastic Sequence Stratigraphy. Am. Ass. Petrol. Geol. Mem., Vol. 3, pp. 449–492.
Wdowinsky, S., Axen, G.J., 1992. Isostatic rebound due to tectonic denudation: a viscous flow model of a layered lithosphere. Tectonics 11 (2), 303–315.
Ziegler, P.A., 1988. Evolution of the Arctic-North Atlantic and the western Tethys. Am. Ass. Petrol. Geol. Mem. 43, 198.